derived age of 3.35 Ma of this event is within the radiometric age uncertainty for our escorias and the astronomically tuned calibrations for the paleomagnetic record.

Consequently, the escorias and tierras cocidas are proposed to be products of a mid-Pliocene impact. The source crater for the Chapadmalal escoria has not been located. Nevertheless, the size of the largest glass bomb (2 m in length) identified thus far is comparable to the largest glasses recovered at other major impact structures (*19*), which suggests an impact in Argentina of similar magnitude. Because the shoreline has eroded inland several kilometers since the Pleistocene, surface expression of any nearshore or offshore structure would have been easily erased.

The distinctive glasses provide a critical isochron for the Pampean Formation, placing better time constraints on faunal evolution in general (*20*). It is intriguing that there is a significant faunal turnover just above the escoria layer, marked by the disappearance of many endemic genera (*13*). Within uncertainties, the radiometric age of the impact glass and paleomagnetic age of the deposits coincide with a pulselike change in the deep-sea stable isotopic record, reflecting a sudden change in climate and ocean circulation. These coincidences suggest that the impact may have directly induced regional faunal extinctions or triggered broader environmental changes leading to ecosystem collapse in Argentina.

References and Notes

1. M. E. Teruggi, *J. Sed. Petrol.* **27**, 322 (1957).
2. M. A. Zárate and A. Blasi, *Quat. Internat.* **17**, 115 (1993).
3. J. C. Heusser and G. Claraz, *Neue Denk. (Nov. Mems.) der Allgemeine Schweiz. Gessell. XXI* **27**, Zurich (1865).
4. Other interpretations for the origin of the escorias include vitrified high-silica sediments produced by early inhabitants or the burning of silica-rich grasses [F. Ameghino, *Anales del Museo Nacional de Buenos Aires* **XIII** (ser. 3a), 39 (1910)], precipitation of chalcedony or opal from silica-rich solutions [C. R. Cortelezzi, *Revista del Museo de La Plata (nueva serie), sección Geología,* **VII**, 233 (1971)], and loess fused by natural fires fluxed with organics [A. Bloom, *Geol. Soc. Am. Abstr. Prog.* **24**, A136 (1992)]. Detailed studies carried out early in this century, however, demonstrated that the escorias could not have been derived from the burning of grasses and sediments due to the necessity for high temperatures (1300°C and 1350°C) and the absence of vegetative remains [F. Outes, E. Herrero Ducloux, H. Bücking, *Rev. Museo de la Plata* **XV**, 1, 138, (1908)]. Because their chemical analyses indicated that the composition of the escorias was identical to volcanic ashes, they classified the scoriaceous escorias and tierras cocidas as andesitic lavas and tuffs.
5. M. A. Zárate and J. L. Fasano, *Palaeogeogr. Palaeoclimatol. Palaeoecol.* **72**, 27 (1989).
6. P. H. Schultz, C. Koeberl, T. Bunch, J. Grant, W. Collins, *Geology* **22**, 889 (1994); P. H. Schultz and R. Lianza, *Nature* **355**, 234 (1992).
7. J. Pohl, D. Stöffler, H. Gall, K. Ernston, in *Impact and Explosion Cratering*, D. J. Roddy, R. O. Pepin, R. B. Merrill, Eds. (Pergamon, New York, 1977), pp. 343–404.
8. D. Stöffler, *Fortschritte Mineral.* **49**, 50 (1972).
9. A. El Goresy, *J. Geophys. Res.* **70**, 3453 (1965). Because baddeleyite rarely occurs in volcanic materials, its use as a good criterion for impact also depends on its occurrence, for example, in a glass matrix entraining other xenocrysts derived from local lithologies and exhibiting distinctive impact glass textures, particularly when out of geologic context for a plausible alternative process (such as a volcanic source or a fulgurite).
10. S. W. Kieffer, *J. Geophys. Res.* **76**, 5449 (1971); R. A. F. Grieve and A. M. Therriault, *Lunar Planet. Sci. XXVI*, 515 (1995).
11. M. Yrigoyen, *Relatorio de Geología de la Provincia de Buenos Aires, VI Congreso GeológicoArgentino* (1975), pp. 139–168. Thick (up to 800 m) Miocene clays with interbedded evaporites underly the loess about 50 km north of the study area.
12. M. A. Zárate, thesis (Museo de la Plata, La Plata, Argentina, 1989).
13. L. Kraglievich, *Rev. Mus. Cienc. Nat. Trad. Mar del Plata* **1 (1)**, 8 (1952). E. Tonni, M. T. Alberdi, J. L. Prado, M. S. Bargo, and A. Cione [*Paleogeogr. Paleoclimatol. Paleoecol.* **95**, 179 (1992)] recognized that the most important turnover recorded in the Chapadmalal Formation occurred between the stratigraphic unit containing the escorias (where 36 genera became extinct and 3 new genera appeared) and the overlying unit. This turnover mostly affected endemic families and genera. Among others, the xenarthrans (for example, Glyptodontidae: *Plohophorous, Trachycalyptus, Plohophoroides*; Mylodontidae: *Proscelidodon*; Dasipodidae: *Doellotatus*), Marsupialia (*Thylacosmilus atrox*), and the native ungulates (*Brachitherium*, a litoptern; *Xotodon*, a toxodontid) disappeared. Also, the last record of the flightless cariamid birds is registered during the Chapadmalalan.
14. These analyses were performed at the Laboratory for Argon Isotopic Research at MIT following procedures described by K. V. Hodges *et al.* [*Contrib. Min. Petrol.* **117**, 151 (1994)]. Fish Canyon sanidine was used to monitor neutron fluence, with an assigned age of 27.95 Ma [P. R. Renne *et al.*, *Geology* **22**, 783 (1994); A. K. Baksi, D. A. Archibald, E. Farrar, *Chem. Geol.* **129**, 307 (1996)], and the J-value for the samples is 0.001439 $\pm$ 0.000008 (2σ). Regressions of data were based on the method of D. York [*Earth Planet. Sci. Lett.* **5**, 320 (1969)].
15. M. J. Orgeira, *Phys. Earth Planet. Lett.* **64**, 121 (1990); J. L. Flynn and C. C. Swisher III [*Geochronol. Time Scales Global Strat. Corr., SEPM Spec. Pub.* **54**, 317 (1995)] estimated that the Chapadmalense spanned a time from 4 to 3.4 Ma, based on correlations between an incomplete section and undifferentiated lithostratigraphic units in Bolivia.
16. The magnetostratigraphic time scale follows F. J. Hilgen [*Earth Planet. Sci. Lett.* **104**, 226 (1991); *ibid.* **107**, 349 (1991)]. The absence of the Kaena subchron within the Gauss reflects locally increased sedimentation rates of loess after the paleosoils developed before the Mammoth subchron.
17. W. Prell, *Science* **226**, 692 (1984); D. Hodell, D. Williams, J. P. Kennett, *Bull. Geol. Soc. Am.* **96**, 495 (1985); D. A. Hodell and J. P. Kennett, *Paleoceanography* **1**, 285 (1986).
18. R. Tiedemann, M. Sarnthein, N. J. Shackleton, *ibid.* **9**, 619 (1994).
19. Suevitic bombs as large as 0.5 m from the 24-km-diameter Ries Crater have been recovered (*10*). Impact glasses as large as 1 m have been recovered from the 14-km-diameter Zhamanshin crater [V. I. Feldman, *et al.*, in *Impactites*, A. A. Marakushev, Ed. (Moscow University, Moscow, 1980), pp. 70–92], and impact glasses as large as 2 m have been recovered from the 18-km-diameter El'gygytgyn crater [V. I. Bouska, P. Povondra, P.V. Florenskij, Z. Rand, *Meteoritics* **16**, 171 (1981)].
20. For example, our new dates for the escoria layer suggest that the chronological boundaries between South American Pliocene stages established by A. Cione and E. Tonni [*J. Soc. Am. Earth Sci.* **9**, 221 (1996)] may have to be revised.

21. We sincerely thank W. Collins and R. Lianza for their unfailing cooperation and support, Fernanda Vicetto for first sharing her small green glasses that led us to the region, and J. Clarke for help in exploring their occurrences. We also thank K. Hodges for access to the MIT $^{40}Ar/^{39}Ar$ geochronology facility and J. Devine for assistance in using the Keck/NSF electron microprobe at Brown University. This research was supported in part by NASA grant NAG5-3877.

28 July 1998; accepted 29 October 1998

The Dusty Atmosphere of the Brown Dwarf Gliese 229B

Caitlin A. Griffith, Roger V. Yelle, Mark S. Marley

The brown dwarf Gliese 229B has an observable atmosphere too warm to contain ice clouds like those on Jupiter and too cool to contain silicate clouds like those on low-mass stars. These unique conditions permit visibility to higher pressures than possible in cool stars or planets. Gliese 229B's 0.85- to 1.0-micrometer spectrum indicates particulates deep in the atmosphere (10 to 50 bars) having optical properties of neither ice nor silicates. Their reddish color suggests an organic composition characteristic of aerosols in planetary stratospheres. The particles' mass fraction (10^{-7}) agrees with a photochemical origin caused by incident radiation from the primary star and suggests the occurrence of processes native to planetary stratospheres.

The past 6 years have provided the first detections of planets and the slightly larger brown dwarfs outside our solar system (*1*, *2*). Among these substellar mass objects, Gliese 229B (Gl229B) is unique: With an effective temperature of 900 K, it is the coolest for which spectroscopic measurements are possible (*1*, *3*, *4*). Gl229B's temperature forces a reduced chemistry (a NH_3, CH_4, H_2O, and H_2 composition), similar to the upper atmospheres of the jovian planets (*5*). Consequently, Gl229B's near-infrared (IR) spectrum (*6*, *7*) is dominated by methane and water fea-

C. A. Griffith, Department of Physics and Astronomy, Northern Arizona University, Flagstaff, AZ 86011–6010, USA. R. V. Yelle, Center for Space Physics, Boston University, 725 Commonwealth Avenue, Boston, MA 02215, USA. M. S. Marley, Department of Astronomy, New Mexico State University, Las Cruces, NM 88003–0001, USA.

tures. The strengths of these features rule out the presence of high-altitude clouds composed of simple ices, such as ammonia and water, present on Jupiter, or the dust that subdues absorption features in the spectra of GD165 and M dwarf stars (*8*). Also revealed by near-IR spectra is a gravity in Gl229B's upper atmosphere 30 to 50 times greater than that of Jupiter (*3*, *4*). The high gravity and the lack of high clouds allow visibility to pressures exceeding 50 bars, an order of magnitude larger than possible on planets in our solar system. Thus, in Gl229B, we have the opportunity to investigate atmospheres in a unique thermodynamic regime.

Initial studies of Gl229B's near-IR spectrum, indicating a particulate-free atmosphere (*3*, *4*), match most spectral features. Yet, these synthetic spectra depart from observations near 1.05 and 1.25 μm, where the brightness temperature is high (1600 K) and emission derives from pressures greater than 30 bars. At wavelengths shorter than 0.92 μm, the primary absorbing gases, methane and water, are comparatively transparent, and observations should probe to the hotter and deeper atmospheric levels. At these wavelengths, an increase in Gl229B's flux was expected. Surprisingly, optical photometry and spectroscopy measured a decrease in Gl229B's flux (*7*, *9*). Simple adjustments to the input parameters of standard models (for example, gravity or effective temperature) do not resolve this discrepancy.

Here, we investigate the structure of Gl229B's atmosphere by analyzing its optical spectrum (0.85 to 1.0 μm) obtained at the Keck 1 Telescope (*7*). Radiative transfer calculations allow us to examine the absorption and scattering of Gl229B's flux, resulting from the native gases and possible particulates (*10*). Initially, we replicate past models of Gl229B's near-IR spectrum (*3*, *4*) with a dust-free calculation containing H_2, He, and water absorption (*10*). This test confirms the original predictions, with a calculated 0.85- to 0.92-μm flux 5 to 80 times greater than that observed (Fig. 1A). In this spectral region, the model provides an atmosphere that is too transparent, yielding excess emission from the hot levels below 200 bars. An unaccounted-for source of opacity must exist in Gl229B's atmosphere.

Several considerations indicate that the missing absorber is neither water vapor nor any other gas. The spectral characteristics of water do not match those required. At 0.93 to 1.0 μm, where water features dominate, the calculated flux lies below the observed spectrum (Fig. 1A), indicating the presence of too much absorption. A smaller water abundance derived from an oxygen composition that is 65% of the solar value fits the overall observed flux level at 0.92 to 1 μm but yields water features deeper than those observed considering the 1σ noise level of 10^{-17} ergs cm^{-2} s^{-1} μm^{-1}. This model also fails to match observations at shorter wavelengths (Fig. 1A), where water is optically thin and does not substantially affect the spectrum. We considered a suite of other gases as potential absorbers, based on the possible mo-

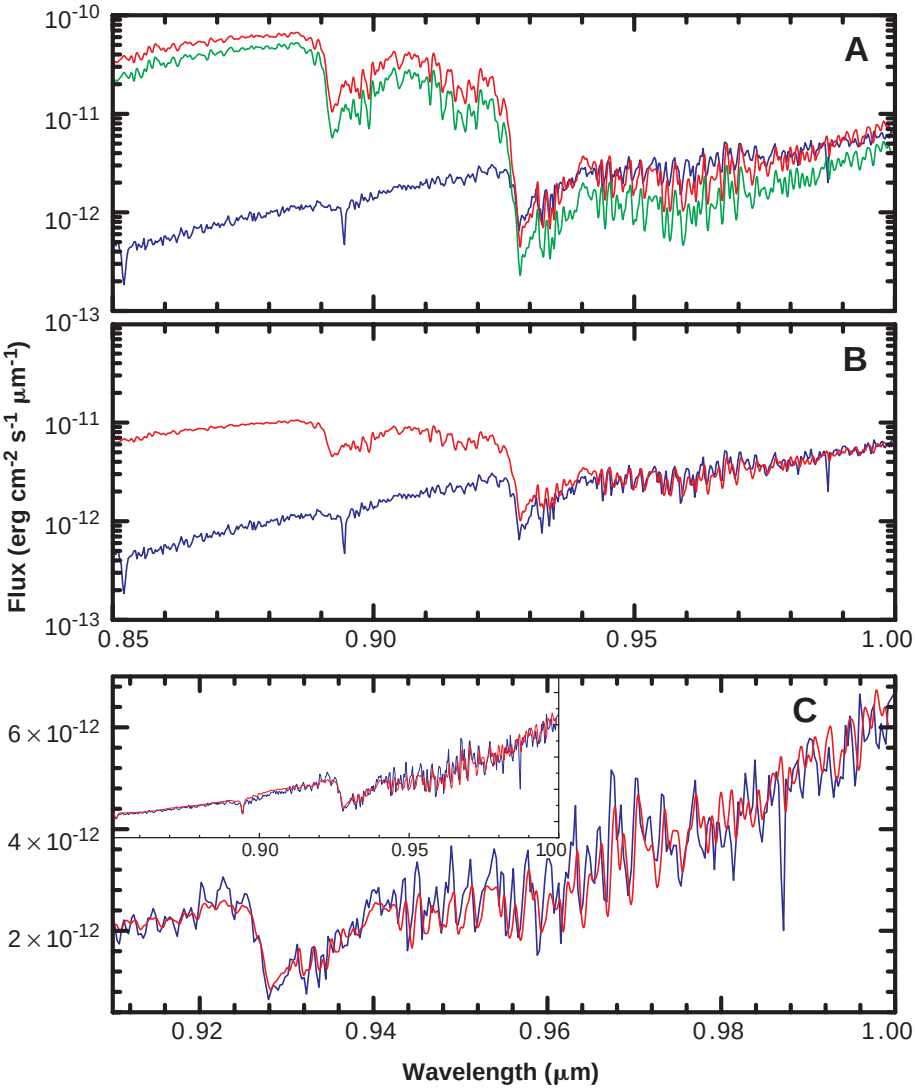

Fig. 1. Models of Gl229B's atmosphere. Blue lines show the Keck spectrum of Gl229B (*7*). (**A**) Synthetic spectra resulting from radiative transfer calculations of Gl229B that assume a particle-free atmosphere. Two water abundances are considered. The solar abundance model (green line) replicates previous calculations used to interpret Gl229B's near-IR spectrum (*3*, *4*). Here, the thermal profile derived for a clear atmosphere was used (*3*, *4*). A water abundance 0.65 times that of the solar model fits the 0.95- to 1.1-μm region; however, it fails to interpret wavelengths shortward of 0.92 μm (red line). In addition, it produces water features deeper than those observed at 0.93 to 1.0 μm. (**B**) An atmospheric model that includes the effects of silicate dust (with $n_i = 0.001$ and $n_r = 1.65$). The haze distribution is defined by $N = 1.6 \times 10^4$ particles per cubic centimeter. This calculation yields a spectrum equivalent to that calculated with iron dust ($n_i = 3$ and $n_r = 4$) for a haze distribution defined by $N = 2.5 \times 10^3$ particles per cubic centimeter. The resultant synthetic spectrum (red line) matches the depths of the 0.93- to 1.0-μm water bands better than do those derived assuming a cloud-free atmosphere. However, this spectrum still fails to fit Gl229B's observations for wavelengths shorter than 0.92 μm. (**C**) An atmosphere having a reddish haze with optical constants adjusted to match the observations (that is, $n_i \leq 0.01$ at 1 μm increasing to 0.1 at 0.9 μm and further to 0.4 at 0.85 μm and $n_r = 1.65$) yields the model spectrum shown (red line). We use a haze distribution defined by $N = 1.6 \times 10^4$ per cubic centimeter. The *y* axis is linear and the *x* axis is enlarged to better exhibit the water features. (**Inset**) Our fit to Gl229B's entire 0.85- to 1.0-μm spectrum.

lecular forms of cosmically abundant elements (for example, N_2, NH_3, CO, CO_2, and CH_4) (*5*), and found that none of these molecules have transitions that produce strong bands at 0.85 to 0.92 μm (*11*).

The remaining candidate for the missing absorber is particulates. Indeed, the opacity source must exhibit no fine spectral structure characteristics of molecular absorption of gases, because none other than water and cesium are indicated in the optical spectrum. In addition, the unidentified constituent must provide substantial opacity throughout the region observed, because the water features are uniformly shallower than those calculated by particle-free atmosphere models (Fig. 1A). Particulates have both of these properties. To test this hypothesis, we incorporated particles into our clear-atmosphere model using three parameters to specify the nature of the haze: (i) the number density of particles at 27 bars (N), (ii) the imaginary index of refraction (n_i), and (iii) the particle radius (a). The scale height of the haze density follows that of the pressure. The top of the haze layer was set at 5 bars on the basis of the strength of the water feature at 0.93 μm, which establishes this upper bound. The bottom of the haze layer was set at 80 bars, because our spectrum is not sensitive to deeper levels (Fig. 2). A lognormal particle size distribution of width 0.1 was assumed on the basis of particle size distributions observed in Earth's atmosphere. With the real coefficient set at $n_r = 1.65$, we modeled most hazes considered for late M dwarf stars and jovian tropospheres and stratospheres. Silicate oxides [for example, enstatite and olivine (*12*)], corundum, and hydrocarbons generally have n_r values of 1.65 ± 0.15. Iron is an exception; we consider this as a special case.

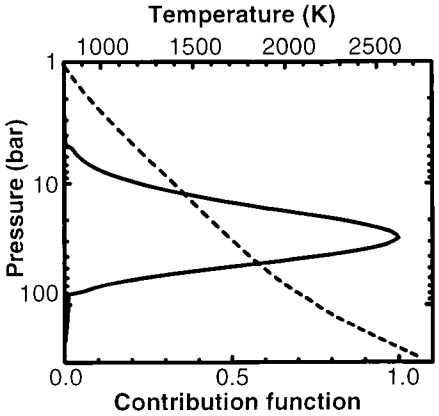

Fig. 2. Contribution function at 0.915 μm, scaled to a maximum value of 1 (solid line, lower *x* axis). Most of the emission originates from the ~14- to 50-bar region. The dashed line (upper *x* axis) shows the pressure-temperature profile derived from Gl229B's observed radiance, assuming radiative convective equilibrium, and the haze distribution that interprets Gl229B's optical spectrum (Fig. 1C). It is radiative above 100 bars and convective below.

At wavelengths less than 0.92 μm, Gl229B's spectrum, mostly insensitive to the water abundance, provides a direct measurement of a possible layer of haze. We constrain the parameter N from the depths of the water features, which are muted in our model by the addition of more haze. The overall flux of Gl229B at 0.85 to 0.92 μm establishes the combined effects of the reflectivity of the haze particles (n_i) and N. At these wavelengths, Gl229B's spectrum indicates a dark material with $n_i = 0.1$ at 0.9 μm, increasing linearly to $n_i = 0.4$ at 0.85 μm. A model atmosphere with $a = 0.1$ μm and $N = 1.6 \times 10^4$ particles per cubic centimeter fits the Keck observations largely within the 1σ noise level of the data (Fig. 1C) (*13*).

At wavelengths less than 0.93 μm, primarily water vapor influences Gl229B's spectrum. When we include the haze distribution described above, a water abundance derived from 30 to 45% of the solar abundance of oxygen is indicated. This subsolar water abundance agrees with recent measurements of the metallicity of Gliese 229A (Gl229A), the companion star of Gl229B (*14*). We find that Gl229B's spectrum requires brightly scattering particles at 0.93 to 1 μm, with $n_i = 0.05$ at 0.93 μm, decreasing linearly to $n_i \leq 0.01$ for wavelengths longer than 0.97 μm. Our haze distribution addresses two independent constraints, the absolute flux and the line depths of the 0.92- to 1.0-μm water features. This model additionally interprets well Gl229B's near-IR spectrum. A more complicated function for n_i is not constrained by our analyses. Yet, this decrease of n_i with increasing wavelength implies a red haze.

The location of Gl229B's haze can be evaluated with a contribution function (*cf*), indicating the strength of emission as a function of pressure:

$$cf(P) = B(\lambda,T)\frac{de^{\tau}}{d\log(P)} \qquad (1)$$

where $B(\lambda,T)$ is the Planck function, τ is the optical depth, and P is the pressure. Particulates reside at altitude levels where detectable flux originates, ~15 to 50 bars. Here, temperatures range from 1400 to 1800 K (Fig. 2).

Studies of stars and planets provide two possibilities for the origin of particulates in the atmosphere of Gl229B. In analogy to Jupiter's troposphere and the photospheres of M dwarfs, they could be cloud particles created by the condensation of refractory species. Alternatively, they could resemble the haze found in planetary stratospheres, produced by photochemical processes acting on the volatile species in the atmosphere. We first consider condensation of refractory grains.

Thermochemical models of Gl229B's atmosphere (*5*) suggest that corundum (Al_2O_3) and grains composed of iron (Fe) and silicates (such as spinel Mg_2SiO_4) form at temperatures >1800 K and are therefore not visible. Compounds containing Si, P, and S may form at lower temperatures; however, these materials are cosmochemically less abundant (*15*). Perovskite ($CaTiO_3$) and other refractory elements condense at temperatures exceeding 1800 K. Although the more refractory grains evidently are present in the photospheres of the coolest M dwarfs (*8*), their condensation levels generally lie at temperatures greater than do the hazes we detect (that is, at higher pressures than present in M dwarfs). Convection could conceivably carry such particles up to the visible atmosphere. However, even when the hazes considered here are included in our model atmosphere calculations (*10*), the atmosphere remains radiative above 100 bars, making it unlikely that abundant refractory grains are carried to the visible atmosphere (*10*, *16*).

A more serious problem with condensation clouds of refractory compounds is the spectral characteristics of these elements. Optical properties of metals and silicates differ from those that we derive for the dust in Gl229B's atmosphere (Fig. 1B). The brown dwarf's low 0.85-μm flux and high 1-μm flux indicate dark red particulates. Iron is dark ($n_i \sim 2$ to 4) throughout the 0.85- to 1-μm region, whereas other known refractory grains (*13*) scatter brightly throughout this region. All these compounds are either gray or blue in color. It has been proposed that red organic material (polycyclic aromatic hydrocarbons) coats particles within red giant stars particularly at temperatures of 900 to 1100 K and in gas environments rich in H_2 and C_2H_2 (*17*). However, this chemistry has not yet been investigated for the more quiescent conditions found within the atmospheres of brown dwarfs.

The optical properties of Gl229B's particulates resemble those of many materials in our own outer solar system. Reflectivities that increase strongly with wavelength and are otherwise featureless appear on the surfaces and coma of comets, planetary satellites, centaurs, some Kuiper belt objects, and the haze in the atmospheres of Titan and the jovian planets (*18, 19*). Most likely, these materials are organic species produced by polymerization of hydrocarbons and nitriles, a process studied most thoroughly for the atmosphere of Titan (*20*). Incident solar ultraviolet (UV) radiation and charged particle precipitation result in the production of nitrogen- and carbon-bearing radicals; subsequent reactions produce species such as C_2H_2 and HCN, which polymerize easily. Laboratory simulations of these processes create solids with optical properties similar to those of

Titan's haze (*21*).

Like Titan, the variety of constituents likely to be present in Gl229B's atmosphere provides a fertile environment for production of photochemical aerosols. Water, CH_4, and CO have been detected in Gl229B, and thermochemical equilibrium calculations suggest the presence of N_2, NH_3, PH_3, and H_2S (*5*). Photochemistry is initiated by the UV flux from the primary star, Gl229A (*20*). The resulting photochemical haze density depends on several processes: (i) the photolysis rate, (ii) the efficiency with which photochemical products are incorporated onto aerosols, and (iii) the rate at which aerosols are removed from the visible atmosphere by mixing and sedimentation. Although insufficient information prevents detailed modeling of these processes, simple estimates are possible.

The UV flux from Gl229A originates in the corona and transition regions of the atmosphere. Because Gl229A's UV radiation has not been measured, we estimate this flux by considering another M dwarf, Gliese 825 (Gl825), that is similar in size and spectral characteristics (*22*). The large equivalent width observed in the Hα features of Gl229A and Gl825 indicates a relatively high pressure in the transition region, where these lines are formed (*23*). The accordingly high column abundance in the corona gives rise to strong emission from the HI recombination continuum. Thus, unlike the sun, where Lyman alpha emission dominates UV radiation, the HI recombination flux governs radiative losses from Gl825. Models that reproduce the observed spectrum of Gl825 predict a UV flux at the star's surface of 3×10^7 ergs cm^{-2} s^{-1} (*22*). We adopt this value for Gl229A, implying a global-average UV flux of 0.04 ergs cm^{-2} s^{-1} incident upon the atmosphere of Gl229B (*24*). This value is comparable to the UV flux of 0.02 ergs cm^{-2} s^{-1} that Titan receives from the sun. If, similar to Titan, one in ten of Gl229A's UV photons results in the production of a molecule with an average mass of 20 atomic mass units that subsequently becomes incorporated in an aerosol, the net mass flux of aerosols is $\phi \simeq 2 \times 10^{-14}$ g cm^{-2} s^{-1}.

The small aerosols deduced from our spectral analysis are removed from the visible atmosphere by eddy diffusion rather than sedimentation. The mass fraction of aerosols (f) is related to the eddy diffusion coefficient K, the mass density of the atmosphere (ρ), and the net mass flux through $f = \phi H/K\rho$, where H is the scale height of the atmosphere (*25*). Because the thermal profile derived for Gl229B (Fig. 2) is radiative, we assume a typical value for K in the radiatively controlled region of planetary atmospheres, 10^3 to 10^4 cm^2 s^{-1} (*26*). When one uses $H = 7$ km, $K = 10^3$ cm^2 s^{-1}, and $\rho = 10^{-4}$ g cm^{-3}, $f = 10^{-7}$ is implied. This value agrees with the mass fraction of haze derived from Gl229B's spectrum. Below the radiating layer, the haze will react with H_2 and reestablish the stable molecular forms of carbon and nitrogen (*27*). Thus, the photochemical production of aerosols is a viable explanation for the haze in Gl229B's atmosphere.

The hypothesis of a deep haze is testable through spectroscopic observations. Isolated brown dwarfs (devoid of the UV flux of a companion star) with effective temperatures near that of Gl229B will presumably lack the dark photochemical haze proposed here. Hence, any such isolated objects should have optical fluxes up to two orders of magnitude larger than that of Gl229B. In addition, along with aerosols, photochemistry produces many simple organic molecules, detected in the atmospheres of Titan and the jovian planets. If found in Gl229B's atmosphere, these disequilibrium species would point to the presence of a photochemical haze. Candidate molecules include those produced primarily by photochemistry (C_4H_2, HC_3N, and CH_3C_2H), rather than molecules that also have other origins, such as C_2H_6 and C_2H_2, which also originate from thermochemistry (*5*).

Our analysis indicates analogies between the atmospheres of the giant planets and those of brown dwarfs. Jovian atmospheres exhibit temperature minima at ~0.1 bar that delineate different atmospheric regions. Above this level (the lower stratosphere), energy is transferred radiatively; photochemistry, instead of thermochemistry, controls the composition and produces aerosols; and the dynamics is quiescent. Below 0.1 bar (the troposphere), energy is transferred by radiation and convection, with the radiative-convective boundary occurring at ~0.5 bar; vertical mixing is more vigorous; and temperatures permit condensation of ices. Below the 2-bar water clouds on Jupiter, cloud-free conditions are predicted until the 1000- to 10,000-bar levels, where iron and olivine condense (*28*, *29*). The temperatures corresponding to this "cloud gap" in Jupiter's interior characterize the temperatures of Gl229B's visible atmosphere.

Our models of Gl229B's spectrum indicate an atmosphere (above 40 bars) that is clear of condensed refractories but contains a red aerosol. We argue that stratospheric processes such as photochemistry, which can produce such a haze, might be expected at high pressures for brown dwarfs. The column abundance above 50 bars on Gl229B corresponds to that above the 0.5-bar level in the Jovian planets. Therefore, radiation from the primary star reaches deeper levels on Gl229B than is possible for planets. Gl229B's large gravity additionally implies a radiative profile down to pressures two orders of magnitude greater than that occurring on Jupiter (*30*). This profile suggests the presence of quiescent stratospheric dynamics that allow particles to survive long enough to "build up" an observable abundance. Gl229B's visible deep atmosphere may consequently resemble the jovian stratosphere, with photochemistry, a radiative profile, and calm dynamics. As such, this brown dwarf represents a laboratory of stratospheric processes at temperatures, pressures, and gravities one to two orders of magnitude greater than those seen on planets in our solar system.

Reference and Notes

1. T. Nakajima *et al.*, *Nature* **378**, 463 (1995).
2. M. Mayor and D. Queloz, *ibid.*, p. 355; G. W. Marcy and R. P. Butler, *IAU Circ. 6251* (1995). Although the first planets and brown dwarfs companioning main sequence stars (like our sun) were detected only recently, A. Wolszczan and D. A. Frail [*Nature*, **355**, 145 (1992)] discovered a planet orbiting a pulsar in 1992.
3. F. Allard, P. H. Hauschildt, I. Baraffe, G. Chabrier, *Astrophys. J.* **465**, L123 (1996).
4. M. S. Marley *et al.*, *Science* **272**, 1919 (1996).
5. B. Fegley and K. Lodders, *Astrophys. J.* **472**, L37 (1996).
6. B. R. Oppenheimer, S. R. Kulkarni, K. Matthews, T. Nakajima, *Science* **270**, 1478 (1995); T. R. Geballe, S. R. Kulkarni, C. E. Woodward, G. C. Sloan, *Astrophys. J.* **467**, L101 (1996).
7. B. R. Oppenheimer, S. R. Kulkarni, K. Matthews, M. H. Van Kerkwijk, *Astrophys. J.* **502**, 932 (1998); A. B. Schultz *et al.*, *ibid.* **492**, L181 (1998).
8. T. Tsuji, K. Ohnaka, W. Aoki, T. Nakajima, *Astron. Astrophys.* **308**, L29 (1996); T. Tsuji, K. Ohnaka, W. Aoki, *ibid.* **305**, L1 (1996); H. R. A. Jones and T. Tsuji, *ibid.* **480**, L39 (1996). Stars within the M dwarf category are the coolest and least massive stars that, like the sun, generate energy from nuclear reactions of hydrogen in their cores.
9. K. Matthews, T. Nakajima, S. R. Kulkarni, B. R. Oppenheimer, *Astron. J.* **112**, 1678 (1996).
10. Our radiative transfer calculation adopts the discrete ordinates technique of K. Stamnes, S. Tsay, W. Wiscombe, and K. Jayweera [*Appl. Opt.* **27**, 2502 (1988)]. Using eight streams, we calculated the thermal emission of the atmosphere with a model that includes Mie and Rayleigh scattering and gaseous absorption. Water absorption accounts for all spectral features except the two cesium lines. We derived absorption coefficients of hot water lines with line-by-line calculations of the water line list determined by H. Partridge and D. W. Schwenke [*J. Chem. Phys.* **106**, 4618 (1997)]. Pressure-induced absorption of H_2 and He was included {following the techniques of A. Borysow and L. Frommhold [*Astrophys. J.* **348**, L41 (1990)] and C. Zheng and A. Borysow [*Icarus* **113**, 84 (1995)]} but, like Rayleigh scattering, is insignificant. Methane also provides insignificant absorption at wavelengths shorter than 0.92 μm and is consequently only considered at longer wavelengths. New, self-consistent, radiative-convective temperature profiles were computed for each distribution of haze considered here. All models assume an effective temperature $T_{eff} = 900$ K and a gravity $g = 1000$ m s^{-2}. Radiative-convective equilibrium calculations followed the techniques described in (*4*) and (*31*). Fluxes, accounting for Rayleigh and Mie scattering, were calculated with the source function approach of O. B. Toon *et al.* [*J. Geophys Res.* **94**, 16287 (1989)].
11. The atmosphere models of (*3*) include the opacities of gaseous diatomic species (TiO and FeH). These absorption features, however, are not detected, consistent with the predicted condensation of these species at levels deeper than those observed (*5*).
12. Optical constants of Fe are given by E. D. Palik [Ed., *The Handbook of Optical Constants of Solids* (Academic Press, New York, 1985)]. Corundum (Al_2O_3) constants calculated from the oscillator parameters are given by C. Koike *et al.* [*Icarus* **114**, 203 (1995)]. Forsterite glass optical constants come from A. Scott and W. Dudley [*Astrophys. J. Suppl.* **105**, 401 (1996)]. See V. Ossen-

kopf, T. Henning, and J. S. Mathis [*Astron. Astrophys.* **261**, 567 (1992)] for silicate minerals.
13. The number density N depends on the particle size (a) assumed, because the optical depth scales as the cross section of the particles, that is, as $(Q_{ext}a^2)^{-1}$, where Q_{ext} is extinction efficiency, calculated by Mie theory. Hazes composed of particles 1 μm in radius and larger fail to produce spectra that match the observations, because they scatter efficiently at 1 μm and diminish the depths of the water features.
14. C. G. Schiavon, B. Barbuy, and P. D. Singh [*Astrophys. J.* **484**, 499 (1997)] measured a metallicity of [Fe/H] = −0.2 ± 0.4 for Gl229A. This result points to a subsolar abundance and yet overlaps the earlier measurement of [Fe/H] = 0.15 ± 0.15 [J. Mould, *Astrophys. J.* **226**, 923 (1987)].
15. This point is also made by (*31*). In M. Marley *et al.*'s (*3*) clear-atmosphere models, the radiative-convective boundary lies below 100 bars.
16. T. Guillot *et al.*, in *Astronomical and Biochemical Origins and the Search for Life in the Universe*, C. Cosmovici, S. Bowyer, D. Werthimer, Eds. (Editrice Compositori, Bologna, Italy, 1997), pp. 343–350.
17. M. Frenklach and E. D. Feigelson, *Astrophys. J.* **341**, 372 (1989); B. J. Cadwell, H. Wang, E. D. Feigelson, M. Frenklach, *ibid.* **429**, 285 (1994).
18. For general discussion and references for specific objects, see T. Owen, D. Cruikshank, C. de Bergh, T. Geballe, *Adv. Space Res.* **16** (no. 2), 41 (1995); C. Matthews, *Origins Life* **21**, 421 (1992); D. P. Cruikshank, *Adv. Space Res.* **7** (no. 5), 109 (1987); *ibid.* **9** (no. 2), 65 (1989); J. R. Cronin, S. Pizzarello, D. Cruikshank, in *Meteorites and the Early Solar System* (Univ. of Ariz. Press, Tucson, AZ, 1988), pp. 819–857.
19. The photochemical formation of polyacetylenes is discussed by Y. L. Yung, M. Allen, and J. P. Pinto [*Astrophys. J. Suppl.* **55**, 465 (1984)]. Photochemical production of haze from cyanoacetylene and cyanoacetylene-acetylene polymers is discussed in (*32*).
20. The UV radiation produced in the upper atmospheres of brown dwarfs is unknown and ignored in this study. Photons energetic enough for photolysis depend on the bonds inherent to the targeted molecule. Several threshold wavelengths [H_2 (0.08 μm), CH_4 (0.135 μm), NH_3 (0.2 μm), H_2O (0.175 μm), and CO (0.088 μm)] indicate that it is the UV radiation of Gl229A shortward of 0.2 μm that drives photochemistry.
21. Recent work on laboratory simulations of organic aerosol formation in planetary atmospheres is summarized by (*32*); P. Coll *et al.* [*Adv. Space Res.* **16** (no. 2), 93 (1995)]; C. P. McKay [*Planet. Space Sci.* **44**, 741 (1996)]; G. D. McDonald, W. R. Thompson, M. Heinrich, B. N. Khare, and C. Sagan [*Icarus* **108**, 137 (1994)]; and B. Khare *et al.* [*ibid.* **60**, 127 (1984)].
22. For Gl229A, the equivalent width of the Hα line has been measured to be 3.6×10^{-5} μm [M. S. Giampapa, L. E. Cram, W. J. Wild, *Astrophys. J.* **345**, 53 (1989)] and 1.1×10^{-4} μm [P. B. Byrne, J. G. Doyle, J. W. Menzies, *Mon. Not. R. Astron. Soc.* **214**, 119 (1985)]. For Gl825, the measured value is 6×10^{-5} μm (E. R. Houdebine thesis, Paris XI, University of Orsay, Orsay, France, 1990). Gl229A emits MgII, CaII, and x-ray emissions of 1.44×10^5, 4.47×10^4, and 3.63×10^4 ergs cm^{-2} s^{-1}, respectively. Gl825 emits MgII, CaII, and x-ray fluxes of 1.95×10^5, 1.12×10^5, and 9.1×10^4 ergs cm^{-2} s^{-1} [P. M. Panagi and M. Mathioudakis, *Astron. Astrophys. Suppl. Ser.* **100**, 343 (1993)].
23. E. R. Houdebine, M. Mathioudakis, J. G. Doyle, B. H. Foing, *Astron. Astrophys.* **305**, 209 (1996).
24. We assume that Gl229B is 40 astronomical units from Gl229A, the distance corresponding to the angular separation between these two objects.
25. This expression applies for K and H constant with altitude. The derivation of and assumptions behind the equation are given by J. W. Chamberlain and D. M. Hunten [*Theory of Planetary Atmospheres* (Academic Press, San Diego, CA 1987)]. This reference also contains information on the thermal profiles of planetary atmospheres.
26. The eddy diffusion coefficient in Earth's lower stratosphere is 5×10^3 cm^2 s^{-1} [J. R. Holton, *J. Geophys. Res.* **91**, 2681 (1986)]. At the 300-mbar level in Jupiter's stratosphere, the eddy diffusion coefficient is $< 4 \times 10^3$ cm^2 s^{-1} [B. J. Conrath and P. J. Gierasch, *Icarus* **57**, 184 (1984)].
27. J. Lewis and B. Fegley, *Space Sci. Rev.* **39**, 163 (1984).
28. Results for the Galileo probe nephelometer experiment reported by B. Ragent *et al.* [*J. Geophys. Res.* **103**, 22891 (1998)] indicate particulates above 0.55 bar, from 0.76 to 1.34 bars, and from 1.9 to 4.5 bars, which are interpreted as NH_3/NH_4SH, and H_2O clouds respectively. B. E. Carlson, A. A. Lacis, and W. B. Rossow [*ibid.* **98**, 5251 (1993)] find that their analysis of mid-IR spectra of Jupiter is consistent with the three thermodynamically predicted cloud layers: the visible NH_3 cloud near 0.5 bar, the NH_4SH cloud near ≈2 bars, and the H_2O cloud near 5 bars. The presence of the H_2O cloud is inferred from the signature of particulates in the IR spectrum. The NH_4SH cloud is inferred from the variation in NH_3 abundance.
29. B. Fegley and K. Lodders, *Icarus* **110**, 117 (1994).
30. There may exist, however, a thin detached convective zone near ~1 bar, depending on Gl229B's gravity [(*4*); K. S. Noll, T. Geballe, M. Marley, *Astrophys. J.* **489**, L87 (1997)].
31. A. Burrows *et al.*, *ibid.* **484**, 499 (1997).
32. D. W. Clarke and J. P. Ferris, *Icarus* **127**, 158 (1997).
33. C. Griffith is supported by an NSF Young Investigator Award and R. Yelle by the NASA Planetary Atmospheres Program NAG5-4426.

2 September 1998; accepted 5 November 1998

Photoemission Evidence for a Remnant Fermi Surface and a *d*-Wave–Like Dispersion in Insulating $Ca_2CuO_2Cl_2$

F. Ronning, C. Kim, D. L. Feng, D. S. Marshall, A. G. Loeser, L. L. Miller, J. N. Eckstein, I. Bozovic, Z.-X. Shen*

An angle-resolved photoemission study is reported on $Ca_2CuO_2Cl_2$, a parent compound of high-T_c superconductors. Analysis of the electron occupation probability, n(k), from the spectra shows a steep drop in spectral intensity across a contour that is close to the Fermi surface predicted by the band calculation. This analysis reveals a Fermi surface remnant, even though $Ca_2CuO_2Cl_2$ is a Mott insulator. The lowest energy peak exhibits a dispersion with approximately the $|\cos k_x a - \cos k_y a|$ form along this remnant Fermi surface. Together with the data from Dy-doped $Bi_2Sr_2CaCu_2O_{8+\delta}$, these results suggest that this *d*-wave–like dispersion of the insulator is the underlying reason for the pseudo gap in the underdoped regime.

A consensus on the $d_{x^2-y^2}$ pairing state and the basic phenomenology of the anisotropic normal state gap (pseudo gap) in high-T_c superconductivity has been established (*1*), partially on the basis of angle-resolved photoemission spectroscopy (ARPES) experiments (*2–5*), in which two energy scales have been identified in the pseudo gap: a leading-edge shift of 20 to 25 meV and a high-energy hump at 100 to 200 meV (*4*). Both of these features have an angular dependence consistent with a *d*-wave gap. For the sake of simplicity in the discussion below, we refer to these as low- and high-energy pseudo gaps, respectively, in analogy to the analysis of other data (*6*). The evolution of these two pseudo gaps as a function of doping are correlated (*7*), but the microscopic origin of the pseudo gap and its doping dependence are still unestablished. Theoretical ideas of the pseudo gap range from preformed pairs or pair fluctuation (*8*) and damped spin density wave (SDW) (*9*), to the evidence of the resonating valence bond (RVB) singlet formation and spin-charge separation (*10–12*). To further differentiate these ideas, it is important to understand how the pseudo gap evolves as the doping is lowered and the system becomes an insulator. We present experimental data from the insulating analog of the superconductor $La_{2-x}Sr_xCuO_4$, $Ca_2CuO_2Cl_2$, which suggest that the high-energy pseudo gap is a remnant property of the insulator that evolves continuously with doping, as first pointed out by Laughlin (*12*).

The compound $Ca_2CuO_2Cl_2$, a half-filled Mott insulator, has the crystal structure of La_2CuO_4 (*13*) and it can be doped by replacing Ca with Na or K to become a high-temperature superconductor (*14*). As with the case of $Sr_2CuO_2Cl_2$, $Ca_2CuO_2Cl_2$ has a much better surface property than La_2CuO_4 and thus is better suited for ARPES experiments

F. Ronning, C. Kim, D. L. Feng, A. G. Loeser, and Z.-X. Shen are with the Departments of Physics, Applied Physics, and Stanford Synchrotron Radiation Laboratory, Stanford, CA 94305, USA. D. S. Marshall is with the Departments of Physics, Applied Physics, and Stanford Synchrotron Radiation Laboratory, Stanford, CA 94305, USA, and Motorola, Phoenix Corporate Research Lab, Tempe, AZ 85284, USA. L. L. Miller is with the Department of Physics, Iowa State University, Ames, IA 50011, USA. J. N. Eckstein and I. Bozovic are at the Ginzton Research Center, Varian Associates, Palo Alto, CA 94304, USA.

*To whom correspondence should be addressed. E-mail: shen@ee.stanford.edu